Journal of Materials Chemistry C

APPLICATION

Plasmonics by design: design principles to structure–function relationships with assemblies of metal nanoparticles

Cite this: J. Mater. Chem. C, 2014, 2, 3077

Daniel E. Gómez,*[ab] Timothy J. Davis[ab] and Alison M. Funston*[c]

Received 16th October 2013
Accepted 22nd December 2013

DOI: 10.1039/c3tc32041c

www.rsc.org/MaterialsC

We present an overview on how a simple and analytical theoretical method, namely the Electrostatic Eigenmode Method (EEM), can be used for designing or interpreting the phenomena that results from plasmon coupling. This presentation is complemented with select examples on our successful application of this theory to experiments highlighting the physical insights obtained.

Introduction

Plasmonics[1–3] is a growing field of research that has had a strong impact in many diverse areas ranging from biological sensing,[4] photo-voltaics,[5] photocatalysis[6,7] to solar water purification[8] and tumour ablation.[9,10] This widely spread impact is partly due to the fact that metal nanoparticles can harvest and confine light energy to sub-wavelength dimensions. This in turn results in enormous energy densities, which can be used for enhancing inherently weak optical processes such as Raman scattering,[11] single photon emission,[12] up-conversion[13] and non-linear optical processes.[14]

A localised surface plasmon resonance is a light-induced collective oscillation of the conduction electrons at the surface of a metallic nanostructure.[15] The frequency at which these oscillations take place is greatly determined by material properties of the nanoparticles such as their composition, geometrical shape and the nature of their chemical environment, allowing thus for systematic tailoring of the optical properties of metal nanoparticles by suitable choice of these experimental

[a]CSIRO, Materials Science and Engineering, Private Bag 33, Clayton, VIC, 3168, Australia. E-mail: daniel.gomez@csiro.au

[b]Melbourne Centre for Nanofabrication (MCN), Australian National Fabrication Facility, Clayton, VIC 3168, Australia

[c]School of Chemistry, Monash University, Clayton, VIC, 3800, Australia. E-mail: alison.funston@monash.edu

Dr Daniel Gomez is an ARC Post-Doctoral Research Fellow at the Materials Science and Engineering division of CSIRO and a Technology Fellow at the Melbourne Centre for Nanofabrication. He completed a PhD in Chemistry at the University of Melbourne, under the supervision of Laureate Prof Paul Mulvaney in 2007, where he studied the optical properties of individual semiconductor nanocrystals. This work was then awarded the Chancellors Price for Excellence in the PhD Thesis in 2008. He worked as a Post-Doc in CSIRO with Dr Timothy Davis where he studied the surface plasmon resonance of interacting nanoparticles. He is currently a staff member of CSIRO working on applied plasmonics.

Dr Tim Davis is a senior principal research scientist at the CSIRO division of Materials Science and Engineering. Dr Davis holds a PhD in experimental physics from the University of Melbourne. Within CSIRO he has contributed to a broad range of research activities including the development of phase contrast imaging using X-rays, machine vision systems, atom optics and atom waveguides, and microfabrication techniques for sensing systems. His current research is in the area of plasmonics for manipulating optical fields at the nano-scale. He is a member of the Australian Institute of Physics, the Australian Optical Society, the American Physical Society and a Senior Member of the Optical Society of America. He holds a senior technology fellowship at the Melbourne Centre for Nanofabrication and honorary positions at the University of Melbourne and Swinburne University of Technology.

variables.[16,17] For instance, rod-shaped metal particles have a large absorption cross section along their longest axis, with a frequency that is correlated to the rod length.[18] When these particles are placed on a semiconductor surface a Schottky barrier is formed at the interface, resulting in nanoscale photodiodes,[19] demonstrating that careful design of plasmonic-based materials can be used as a platform for creating novel electro-optical devices at the nanoscale.

In this *Applications paper* we describe our approach to plasmonic materials design which consists of a simple formulation of the electrostatic Maxwell equations that govern light–matter interactions of metal nanoparticles. We provide experimental evidence that supports the validity of our theory and furthermore, we demonstrate how one can achieve simple structure–property relationships that can aid in the design of complex plasmonic structures. As a starting point, in the next section we present a compact overview of the existing experimental methods for creating assemblies of metal nanoparticles. This is followed by examples of how we have used our theoretical method to understand structure–function relationships, such as self-interaction between plasmonic nanoparticles and a substrate, self-assembled nanoparticles and their interactions with light, optical dark modes and interfering resonances leading to a plasmonic ruler.

Nanoparticle assemblies and plasmonic coupling

Metal nanoparticles and their assemblies are generally formed either lithographically (the top-down approach) or *via* chemical colloidal synthesis (the bottom-up approach). Particles fabricated lithographically are relatively uniform-sized plates with a designed 2-dimensional shape. One of the key advantages of this approach is that it allows for an accurate 2D and 3D positioning of these particles within complex assemblies. However, the resulting nanoparticles are multi-crystalline with some surface roughness and grain boundaries.[20–22]

Particles colloidally grown are single or twinned crystal structures, with smooth facets. Their three-dimensional geometry is controlled by synthesis conditions and ligands. However, colloidal samples contain a random distribution of both crystal sizes and shapes. While the percentage yield of a desired crystal geometry can often be optimized for a given set of experimental parameters, in many cases this yield does not approach 100%. Bottom-up approaches for the creation of nanoparticle superstructures rely on the assembly of pre-synthesised colloidal nanocrystals into discrete structures *via* chemical linkers (for an in-depth discussion see ref. 23). The vast majority of linking molecules for self-assembly of metal nanoparticles contain thiol (or dithiol) functional groups, due to the strong affinity of thiols for gold surfaces and colloids. The two key advantages of chemical self-assembly over the top-down approach are the high throughput and the short inter-particle distances attainable (on the order of a molecular length!) which is deemed to be beneficial for achieving strong plasmonic coupling.[24]

The resulting plasmonic assemblies fabricated by either approach have unique optical properties. In Fig. 1 we show the light scattering spectra measured for a set of assemblies containing a pair of Au nanorods.[25] It is clear that the geometrical arrangement of these two nanorods plays a significant role in determining the light-scattering spectra. Blue and red-shifts in

Dr Alison Funston is a lecturer and Future Fellow in the School of Chemistry at Monash University, Melbourne, Australia. Dr Funston received her PhD from The University of Melbourne, Australia, in 2002. After working as a postdoctoral fellow at Brookhaven National Laboratory with Dr John Miller in the areas of electron transfer and radiation chemistry, she returned to The University of Melbourne where she worked with Prof. Paul Mulvaney in the spectroscopy of nanoscale systems. She moved to Monash as a lecturer in 2010 and was awarded an ARC Future Fellowship in 2011. Her research focuses on the energy transport and optical properties of well-defined assemblies of nanoparticles, including metal nanocrystals and semiconductor nanocrystals, as well as charge and energy transfer within nanoparticle–organic systems.

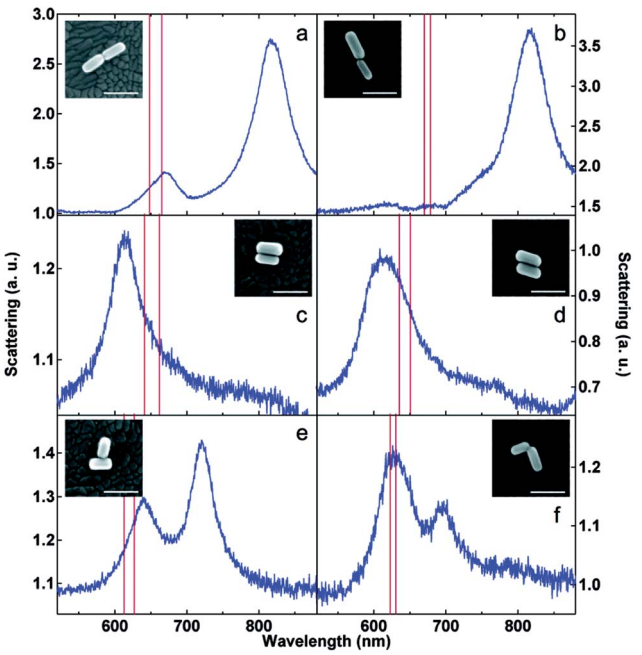

Fig. 1 Scattering spectrum for two gold rods aligned (a and b) end-to-end, (c and d) side-to-side, (e) in a T configuration, and (f) in an L configuration, all on ITO and in air. The red vertical lines represent the expected position of the longitudinal plasmon resonance for noninteracting single particles of identical dimensions to the rods in that specific dimer. Insets show the SEM images of the particles giving rise to each scattering spectrum. Scale bar = 100 nm. (Reproduced with permission from the American Chemical Society.[25])

the scattering spectra can be observed and the obvious explanation is that as a result of their close proximity, plasmonic coupling effects are responsible for these observations. In the next section we present a theoretical model that can describe these observations accurately, providing a simple and intuitive picture for designing systems of coupled plasmonic assemblies.

Electrostatic eigenmode approximation

The optical properties of nanocrystal assemblies can be modelled using numerical approaches[26] such as the discrete dipole approximation,[27] the finite difference in the time domain method (FDTD)[28] and the boundary element method (BEM),[29,30] in addition to the plasmon hybridisation theory, an analogue to molecular orbital theory.[31] However, numerical approaches do not give an in-depth understanding of the underlying physics of the interactions. Here we focus on the Electrostatic Eigenmode Method (EEM), a powerful semi-analytical method that combines the advantages of a relatively short calculation time along with significant physical insight into the underlying physics.

The EEM is a theoretical approach for describing the optical properties of metal nanoparticles and their assemblies (such as those referred to in the previous section and shown in Fig. 1) that uses approximate forms/solutions to Maxwell's equations.[29,30,32,33] The most fundamental approximation made in the EEM is that the nanoparticles and their assemblies are much smaller than the wavelength of light that drives the plasmon resonances.[29,30,32–34,66] The key concept of the EEM, is that the surface plasmon resonances of nanoparticles are described in terms of eigenmodes: self-sustained surface charge oscillations that occur at the surface of the particles.[35] The geometrical shape of the nanoparticle dictates the type of modes that the particle can support. For instance, the eigenmodes of a spherical nanoparticle are shown in Fig. 2, where it can be seen how these resemble the p (for which $l = 1$) and d (for which $l = 2$) atomic orbitals of electrons in atoms.

Each eigenmode has an associated eigenvalue, which in turn predicts the wavelength at which each mode is resonant, once the chemical composition of the particle and its surrounding medium are specified. The first two eigenmodes (γ) of a sphere are $\gamma = 3$ and $\gamma = 5$ (as shown in Fig. 2), which will have associated resonances at frequencies $\omega_{p,m}$ that satisfy the following relationship:

$$\mathrm{Re}\varepsilon(\omega_{p,m}) = \left(\frac{1+\gamma}{1-\gamma}\right)\varepsilon_b, \quad (1)$$

with $\varepsilon(\omega)$ the (complex) metal permittivity and ε_b the permittivity of the surrounding medium. For $\gamma = 3$ this equation reduces to the well known Fröhlich resonance condition: $\mathrm{Re}\varepsilon(\omega_{p,m}) = -2\varepsilon_b$, that correctly predicts the position of the plasmon resonance of small (when compared to the wavelength of the incident beam of light) spherical metal nanoparticles.

In addition to the eigenvalue and eigenmode concepts, the EEM also takes into account how these modes couple to light by the introduction of excitation amplitudes. For a nanoparticle **a**, photo-excitation results in an oscillating surface charge distribution $\sigma(\vec{r})$ which can be written in terms of the eigenmodes $\sigma_a^m(\vec{r})$ of the particle according to: $\sigma(\vec{r}) = \sum_m a_a^m(\omega)a_a^m(\vec{r})$, where $a_a^m(\omega)$ are the *excitation amplitudes* which describe the strength of the interaction between the incident light field with a particular eigenmode (here m is an index that indicates the m-th mode sustained by particle a). These excitation amplitudes are in general given mathematically by the product of a function $f(\omega)$ accounting for the wavelength-dependence of the resonance and a term that takes into account the relative alignments of the incident polarization of light and the dipole moment of the eigenmode.

Fig. 2(b), shows how the function $f(\omega)$ varies with wavelength for the first three eigenmodes of an Au nanosphere. Each eigenmode has a distinct resonance frequency given by eqn (1). However, only those modes with strong dipolar character couple strongly with uniform electric fields and have thus large values of $a_a^m(\omega)$. For instance, for small metallic nanospheres, only the $l = 1$ ($\gamma = 3$) modes of Fig. 2 have a net dipole moment, and consequently, only these modes have non-vanishing values of $a_a^m(\omega)$. The net result is that the optical spectrum predicted by the EEM (light scattering, absorption) can be interpreted as the light-driven excitation of a superposition of all three degenerate dipolar plasmon resonances of the sphere, which will result in a lineshape such as the one associated with $\gamma = 3$ of Fig. 2(b). Other geometries are considered in Fig. 2(c), which depicts the eigenmodes and their associated resonance frequencies (in eV) when the nanoparticles are made of Au.

The beauty of the EEM is that one can interpret the optical properties of *assemblies of nanoparticles* in terms of simple linear superpositions of the eigenmodes of the isolated nanoparticles, much in the same spirit as in the concept of hybridization of orbitals employed in the description of the chemical bond.[31,36,37] For an assembly of metal nanoparticles, photo-excitation results in a collective plasmon resonance, described by a surface charge density $\sigma(\vec{r})$ which results from the hybridization of the eigenmodes of the uncoupled nanoparticles: $\sigma(\vec{r}) = \sum_{a,m} \tilde{a}_a^m(\omega)\sigma_a^m(\vec{r})$, where contrary to the single-particle case: (i) the sum is now carried out for all the members of the assembly and (ii) the excitation amplitudes $\tilde{a}_a^m$ account for the effect of coupling as we now describe.

Within the EEM, the effect of inter-particle interactions on the excitation amplitudes is mathematically described by a matrix multiplication involving a coupling matrix $\mathbb{C}$ that contains in its non-diagonal elements, a set of coupling coefficients that contain all the details about the inter-particle interactions:

$$\tilde{a} = \mathbb{C}^{-1}a, \quad (2)$$

here a are the excitation amplitudes of the isolated nanoparticles.

Coupling of the localised surface plasmons of two nanoparticles can be interpreted as a Coulomb-type interaction

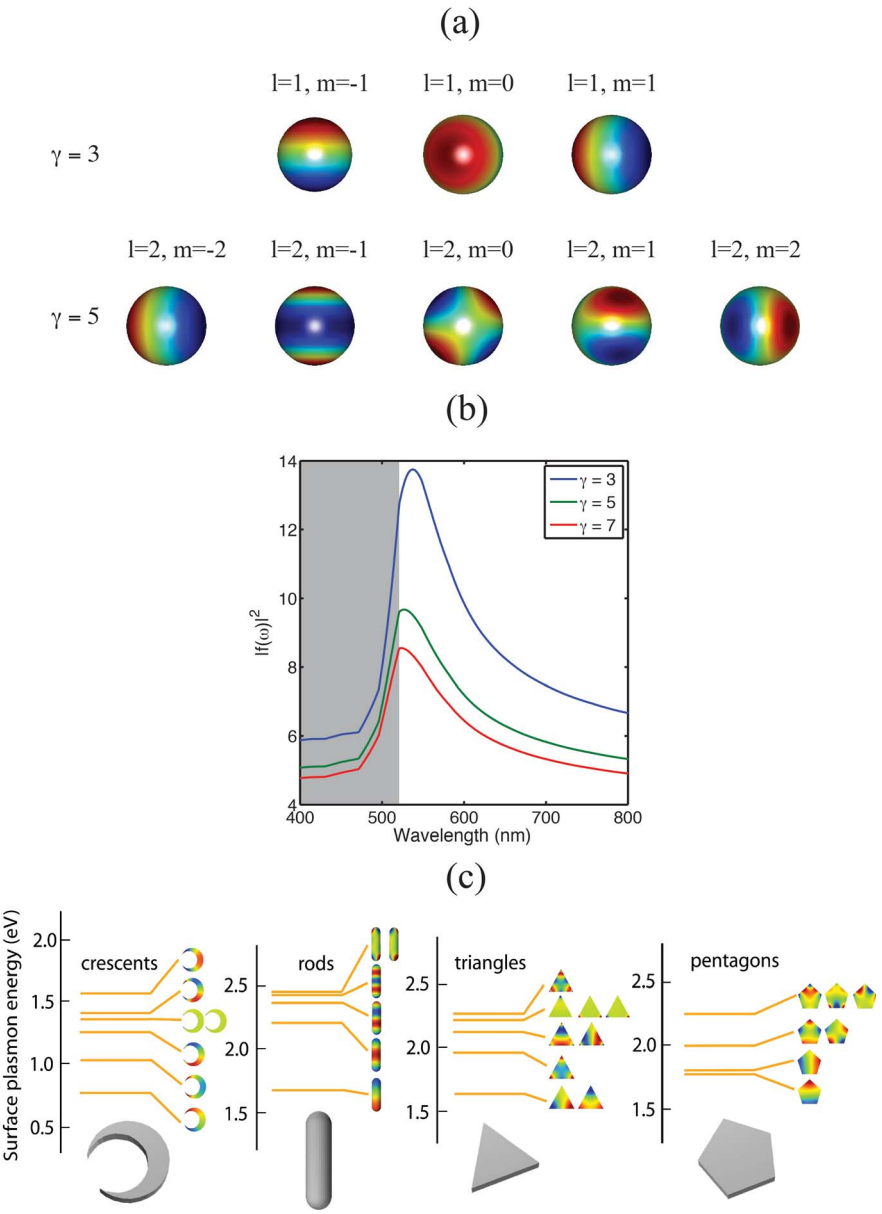

Fig. 2 Surface plasmon modes of a sphere. (a) Plots of the surface charge distributions of the eigenmodes of a sphere with $\gamma = 3$ and $\gamma = 5$. The colors indicate the relative sign of the charges. The indices l and m are used for differentiating the modes. Modes with different values of m but same value of l are degenerate. The modes with $l = 1$ resemble the atomic p orbitals and are the only modes of a sphere with a net dipole moment. (b) Plot of the spectral function $f(\omega)$ that describes the wavelength dependence of the eigenmodes. The shaded area corresponds to the region of interband transitions in Au (dielectric data taken from ref. 65). (c) Examples of the localized surface plasmon modes and their energies for different gold nanoparticles calculated using the EEM. The nanoparticles are assumed to be in a medium with an electric permittivity similar to that of water $\varepsilon_b = 1.75$. (Reproduced with permission from the American Chemical Society.[35])

between their eigenmodes, where the strength of the interaction of two particles a and b can be quantified by a coupling coefficient $C_{ab} = -f_a(\omega)G_{ab}$[35,38] with ω the frequency of light impinging the particles and G_{ab} a dimensionless quantity (real number) accounting for the geometrical details of the arrangement between the particles. To lowest-order, this geometrical factor can be expressed as a dipole–dipole coupling term:[35] $G_{ab} \propto d^{-3}[3(\vec{p}_a\cdot\hat{d})(\vec{p}_b\cdot\hat{d}) - (\vec{p}_a\cdot\vec{p}_b)]$, where d is the interparticle distance and $\vec{p}_{a,b}$ are the dipole moments ($\hat{d}$ is a unit vector along the line separating the particles). From this equation, we see that the geometric coupling is symmetric, $G_{ab} = G_{ba}$, and has a sign that depends on the relative orientation of the dipole moments and on the displacement of the nanoparticles.

In Fig. 3 we show some representative examples of how the coupling matrix is constructed for different nanoparticle assemblies. For a dimer, due to mirror symmetry there is only one coupling coefficient. Solution of eqn (2) for this case is very simple and it reads:

$$\begin{pmatrix}\tilde{a}_1\\ \tilde{a}_2\end{pmatrix} = \frac{1}{\Delta}\begin{pmatrix}1 & C\\ C & 1\end{pmatrix}\begin{pmatrix}a_1\\ a_2\end{pmatrix}, \quad (3)$$

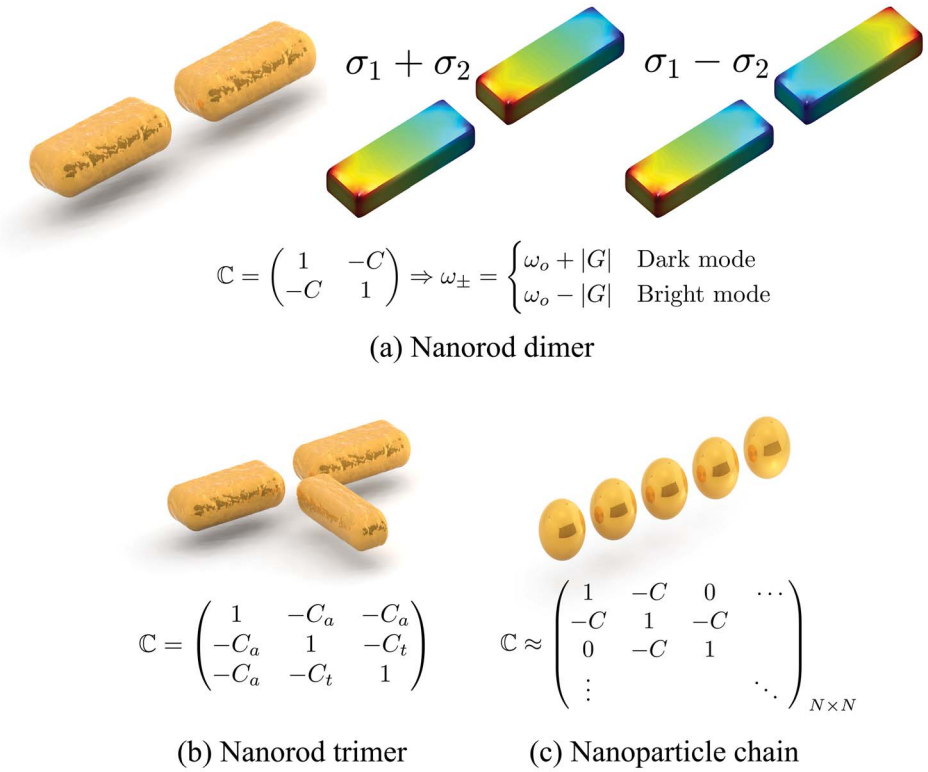

Fig. 3 Some configurations and their associated coupling matrices.

with $\Delta = 1 - C^2$ the determinant of the coupling matrix. The scattering spectrum of this dimer is proportional to $1/|\Delta|^2$ a quantity that will exhibit a maximum when Δ approaches zero or equivalently when $1 = C^2$. We have previously shown[35] that this condition can be written as:

$$1 = C^2 \approx \left(\frac{G}{\omega - \omega_o + i\Gamma_o/2} \right)^2, \quad (4)$$

where ω is the frequency of the light incident on the dimer, ω_o the resonance frequency of each isolated nanoparticle and Γ_o the linewidth of the plasmon resonance. This condition results in two resonance frequencies $\omega_\pm = \omega_o \pm |G|$, which correspond to the two hybrid plasmon modes shown in Fig. 3(a), namely the bright (bonding) mode and the dark (anti-bonding) mode. Only the bright mode has a net dipole moment and is the one that will be excited with, for instance, linearly polarised light. The measured scattering spectrum from such a dimer will therefore consist of a spectral band that is red-shifted from that of the individual particles.

Similarly, it is possible to construct the coupling matrix for more complex geometries. For the trimer of Fig. 3(b), due to mirror symmetry along the axis defined by the longest nanorod, the coupling matrix only contains two different coupling coefficients: one C_a describing the coupling of the long particle (located on the axis of symmetry) to each of the other two and another C_t accounting for the coupling of the two particles lying perpendicular to the mirror axis. One-dimensional chains of particles have also been described by using this simple construction[39] where, as shown in Fig. 3(c), the coupling matrix becomes tri-diagonal and requires only one coupling coefficient (nearest-neighbour coupling). In both of these cases, a detailed analysis based on these coupling matrices and eqn (2), yields all the information required to predict the optical properties of these nanoparticle assemblies.

In spite of its simplicity, the EEM is remarkably accurate and to date, it has been successfully used to interpret the effect of the substrate on the resonances of metal nanoparticles,[40] the intricate inter-connection between relative 3D orientations and the plasmon resonances,[38] the generation of optical chirality,[41,42] the ability of nanoparticles assemblies to have directional light scattering,[43] the interaction of these particles with molecules,[44] with Raman-active species[45] and with active media,[46] as well as the optical excitation of collective dark modes.[47] It is important to recognize that the EEM theory is strictly only valid for very small particles where retardation effects are negligible.[34] However, the method captures much of the essential physics of resonances and coupling which enable useful physical insights. In the next sections we review a few successful examples of how the EEM has aided either the interpretation of experimental results or the design of plasmonic assemblies with targeted optical properties.

"Self-coupling": the substrate effect

The presence of an underlying substrate of different permittivity compared to the rest of the nanoparticle (which may be

immersed in air, ligand or a solvent) affects the frequency of the localised surface plasmon resonance (LSPR). The non-homogeneous environment of a particle on a substrate is the most basic example of nanoparticle coupling: that of itself with its image charge projected in the substrate.

The oscillating surface charge of a plasmon resonance and its associated electric field, polarises the substrate inducing additional surface charges (a mirror charge) at the interface between the substrate and the surrounding medium, as illustrated in Fig. 4(a). The electric field from the image charge then interacts with (couples to) the nanoparticle leading to a shift in the frequency of the LSPR. Experimentally, this effect is manifest as spectral band splitting[48] in addition to spectral shifts.[49] The extent to which the self-coupling affects the LSPR of a given nanoparticle depends on parameters such as the shape and orientation of the nanoparticle as well as on the asymmetry of the dielectric permittivities of the environment of the nanoparticle.

Theoretically, the effect of the substrate on the plasmon resonance of metal spheres can be taken into account by first principles calculations[16,26,50] or by full numerical solutions of Maxwell's equations.[48] However, application of the EEM to this problem allows for significant insight into the physical mechanisms underlying the particle–substrate interaction along with providing a general theory for particles of arbitrary shape supported on a substrate.[40]

Within the EEM formulation of this problem, the induced image charge of the nanoparticle is considered to be a pseudoparticle and therefore the effect of the substrate on the plasmon resonance is analysed as a two-particle coupling situation. This interaction modifies the excitation amplitude of the nanoparticle much like the cases considered in relation to Fig. 3(a). In this case however, the coupling coefficients describe the coupling strength for the particle with its image charge and are proportional to the fractional difference in dielectric permittivities between the two media surrounding the nanoparticle.

The most salient feature of our application of the EEM to this simple self-coupling problem is the fact that it can be recast in a much simpler way: the nanoparticle is embedded in a uniform medium with an effective permittivity, as shown in the diagram of Fig. 4(b). This effective background permittivity is written as a semi-analytical expression which incorporates all of the phenomenology of the self-coupling from first principles but in a very tractable way.[40] The predictions of this method are comparable to experimental data for the interesting case of gold nanorods with increasing aspect ratios. As the aspect ratio of the nanorod increases, the strength of the nanorod–substrate interaction decreases, however the metal permittivity increases more rapidly resulting in an overall (nonlinear) increase in the effective permittivity as a function of aspect ratio.[40] The EEM also predicts the observed spectral mode splitting.[48] Having presented this simple case, in the next section we illustrate how the EEM can be used for interpreting the optical spectra of assemblies of metallic nanoparticles.

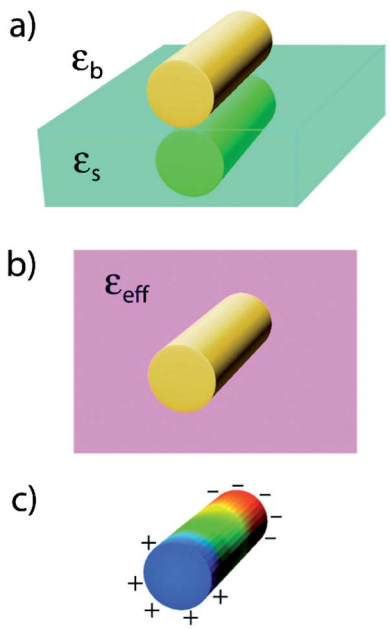

Fig. 4 (a) The particle on a substrate and its mirror image that acts as a pseudoparticle, where ε_b is the dielectric permittivity of the surrounding environment and ε_s is that of the substrate. According to the method discussed in this paper, this system can be mapped into (b) a particle in a homogeneous medium of permittivity ε_{eff}. (c) The surface charges of a nanorod with a predominantly dipolar mode. (Reproduced with permission from the American Chemical Society.[40])

Colloidal self-assembly

Colloidal self-assembly of designed nanocrystal superstructures has evolved sufficiently for the formation and optical interrogation of simple one-dimensional,[25,39,51] two-dimensional[52–55] and even three-dimensional[56] discrete structures. It should be noted however that without extensive purification steps, self-assembly yields are typically very low, necessitating the use of correlation techniques combined with single particle spectroscopy.[52,57]

In this section we show how the EEM has been used to gain physical insight into two types of these colloidal superstructures. The first case consists of the nanorod dimers shown in Fig. 1. The tip-to-tip configurations of Fig. 1(a) and (b), were considered in Fig. 3(a), where the prediction was the observation of a red-shifted longitudinal surface plasmon resonance, in agreement with the experimental evidence. Similar calculations were carried out for the additional nanorod dimer geometries presented in Fig. 1 using appropriate coupling matrices.[25] In particular, the EEM analysis led to the important conclusion that of the "L"- and "T"-shaped dimer geometries shown in Fig. 1(e) and (f), the "L" geometry has greater plasmon delocalisation throughout the structure, with implications for nanoparticle junctions.[25] Application of the EEM to self-assembled nanorod trimers,[55] with geometries similar to that shown in Fig. 3(b) provided a more complex test of the method. The trends in plasmon resonance energy predicted by calculations agreed well with the experimental data, allowing the identification of modes, and the relative intensities of the

peaks. The trimers investigated experimentally and *via* EEM included extended forms of the "L" and "T" dimers, further confirming the degree of delocalisation in nanorod junctions with these geometries.[55]

As a second general example, we now turn our attention to one-dimensional nanosphere chains with up to $N = 6$ nanoparticles. These chains were formed *via* DNA-based self-assembly methods using simple, but complementary oligonucleotide strands.[39] The DNA coupling scheme was designed to self-assemble structures with small interparticle separations, with the nanoparticles in primary ligand contact. This approach results in chains such as the ones presented in Fig. 5(A).[23] The dark-field scattering spectra of these chains red-shifted significantly as the number of nanoparticles increased.

The EEM method here was applied in the nearest-neighbour approximation as per the diagram of Fig. 3(c), involving a single coupling coefficient and leading to the results shown in Fig. 5(B). This simple approximation identified the red-shifted plasmon resonance as the longitudinal coupling mode, with the plasmon delocalised across all nanoparticles up to $N = 6$. The energy of the coupled mode, both experimentally and as modelled *via* EEM approaches a plateau with increasing N, with little change in the energy predicted after 12 nanoparticles. The asymptotic value was found to be dependant upon the nanoparticle geometry, the dielectric environment of the nanoparticles and the magnitude of the coupling constant, C. A greater agreement between the energies obtained *via* EEM and the experimentally obtained resonance energies was achieved by the adaptation of the EEM coupling matrix to include perturbations caused by higher-order multipole interactions utilising an "effective" dipole–dipole coupling matrix, highlighting the importance of higher-order coupling at these small interparticle separations.[39]

Larger interparticle separations, along with longer chain lengths are able to be achieved for crystalline nanoparticles using a combination of bottom-up and top-down techniques.[58] The individual nanoparticles within the one-dimensional arrays were pentagonal prisms. The magnitude of the calculated energy shift *via* EEM for the pentagonal prisms was similar to that for the equivalent spherical and cylindrical nanoparticle geometry. This is understood by recognizing that, the coupling matrix is algebraically identical for all of these cases and the energy offset arises due to differences in energy of the individual particles individual particles as a result of the different particle geometries.[58]

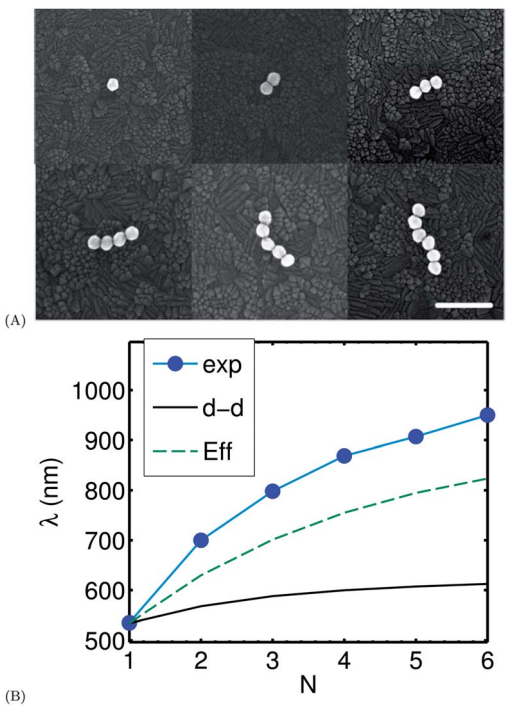

Fig. 5 (A) SEM images of self-assembled nanoparticle chains. Mean diameter of gold particles is 64 nm. Interparticle spacings are estimated at 1 nm. Scale bar = 250 nm. (B) Plot of the surface plasmon resonance (nanometers) as a function of the number of particles, N in a linear chain. The experimental data are shown labelled exp; the calculated response using the EEM are shown for a dipole–dipole coupling limit (d–d) and an effective coupling approximation that incorporates multipolar coupling. (Adapted from ref. 39 with permission from the American Chemical Society.)

Dark modes

In this section we show how one can use the EEM to design a nanoparticle assembly that exhibits a plasmonic dark mode and furthermore, we show how the EEM predicts under which experimental conditions this dark mode can be observed. Plasmonic dark modes (or sub-radiant modes) are those which lack a net dipole moment and are thus able to store electromagnetic energy more efficiently than modes with dipolar character (bright modes) due to an inhibition of radiative losses. These modes are experimentally characterised by possessing narrower spectral line widths a favourable attribute for biochemical plasmonic sensing, or for novel opto-electronic plasmonic devices.

The starting point in designing a plasmonic structure that exhibits a dark mode is to construct the coupling matrix for the assembly of interest. For the equilateral triangular structure of Fig. 6, eqn (2) takes on the following simple form:[37]

$$\begin{pmatrix} \tilde{a}_1 \\ \tilde{a}_2 \\ \tilde{a}_3 \end{pmatrix} = \begin{pmatrix} 1 & -C & -C \\ -C & 1 & -C \\ -C & -C & 1 \end{pmatrix}^{-1} \cdot \begin{pmatrix} a_1 \\ a_2 \\ a_3 \end{pmatrix}, \quad (5)$$

where $a_{1,2,3}$ are the excitation amplitudes of particles 1, 2 and 3, whereas $\tilde{a}_{1,2,3}$ are the excitation amplitudes modified by the inter-particle interactions. Only a single coupling coefficient C is required to describe the D_{3h} symmetric trimer. This is purely a consequence of the symmetry of this arrangement: there is a C_3 axis of rotation, meaning that a rotation of $\pi/3$ around a Z axis located at the centre of the trimer (perpendicular to the page), leaves the assembly unchanged. Therefore the coupling strength of particle 1 (arbitrarily labelled so) to the other two particles should be equal to the other possible interactions.

A simple solution to eqn (5) predicts that the three lowest-energy plasmon modes are those that span the irreducible representations of the point group D_{3h}:[37,59] $A_1' + E'$, where A_1'[67] is a

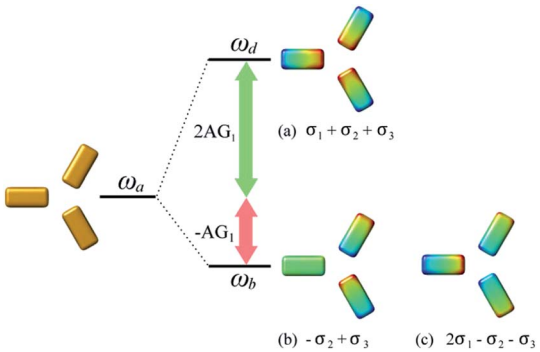

Fig. 6 Collective SP modes of the D_{3h}-symmetric configuration of nanorods. The mode corresponding to the A' representation is a dark mode of the structure.[37] (Reproduced with permission from the American Chemical Society.[47])

representation of D_{3h}, symmetric with respect to a rotation of 120° on the Z axis and E' a two-dimensional representation of this group that is anti-symmetric with respect to a 180° rotation perpendicular to the plane containing the nanorods. These modes are (the eigenvectors of the coupling matrix of eqn (5)) given by the eigenmode hybridizations of Fig. 6.

The doubly degenerate bright modes of the irreducible representation E', are red-shifted in frequency from the plasmon mode of the uncoupled rods and are characterised by the surface charge distributions of Fig. 6(b) and (c). The other eigenmode is the "dark mode" which corresponds to the A' representation of the D_{3h} point group. This mode will have a resonance frequency that is blue-shifted relative to that of the non-interacting nanorods.[47] Noteworthy is the fact that the surface charge distribution of the dark mode shown in Fig. 6(a) has radial symmetry and consequently, can be excited by a radially polarized light beam.

Therefore the predictions of the EEM are: (i) the scattering spectrum of a D_{3h} symmetric trimer under linearly polarised illumination consists of a spectral band red-shifted from that of the one observed for the isolated nanoparticles and (ii) there is a dark mode, accessible by photo-excitation with radially polarised light which will have a spectral band blue-shifted in relation to the isolated nanoparticles.

We have verified these predictions by creating D_{3h}-symmetric trimers through electron-beam lithography and optically interrogated their scattering spectra with linear, radial and unpolarised light. The results shown in Fig. 7 indeed agree with the EEM predictions, indicating once more how this simple theory helps in achieving plasmonic properties (in this case a dark mode) by design. Up to his point we have reviewed cases of planar assemblies of metal nanoparticles. In the next section we illustrate the applicability of the EEM for analysing the complex case of inter-particle interactions in complex three-dimensional structures.

3D plasmonic ruler

As a final example of a more complex structure, we now turn our attention to the three-dimensional plasmonic ruler introduced by Liu *et al.*[60]

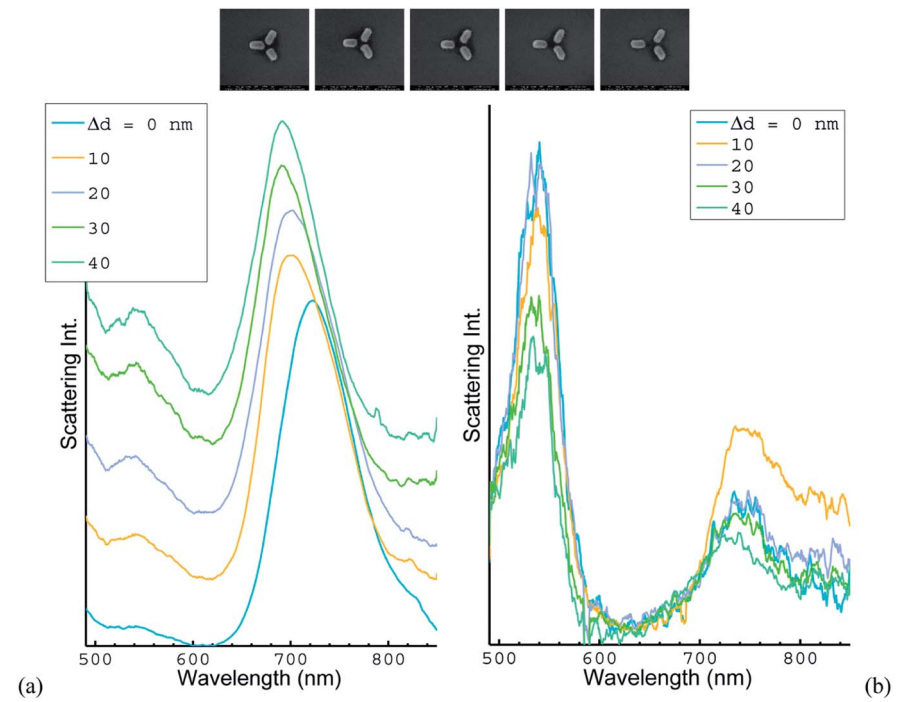

Fig. 7 Plasmonic dark modes of a nanorod trimer. (a) Spectra measured with unpolarized light (b) with radially polarized light. The latter shows a clear band to the blue of the spectrum which is due to the optical excitation of the collective dark mode A_1' of Fig. 6. Symmetry breaking, as shown in the SEMs (achieved by horizontal displacement of one rod) allows for the excitation of this dark mode with unpolarised light as shown in (a) by the appearance of a band at ~550 nm (reproduced with permission from the American Chemical Society[47]).

This structure contains two vertically displaced pairs of metal nanorods and a fifth nanorod placed centrally between them and oriented at right angles. The incident light is polarised parallel to this central rod, which acts as a resonant dipole antenna. No resonances are excited directly in the two pairs of nanorods because of their perpendicular orientation. However, due to plasmon coupling, non-radiative resonances are excited in these nanorods. The loss of energy from the antenna is observed in the scattering spectrum from the structure. The strength of the LSP coupling to the two pairs of nanorods depends on the relative location of the central antenna. Changes in the position of the antenna in two dimensions, vertically and horizontally, are observed by changes in the scattering spectrum.

This is a complex structure that exhibits multiple resonances. However, the EEM has been used to successfully model the scattering spectrum.[38] The matrix coupling equation is greatly simplified by taking advantage of the symmetry of the three-dimensional plasmon ruler. For example, the coupling between the antenna and the lower pair of nanorods are approximately equal but opposite, $C_{a1} = -C_{a2}$ whereas the coupling between the lower pairs themselves are equal, $C_{12} = C_{21}$. Following this through for the other coupling coefficients leads to the following equation:

$$\begin{pmatrix} \tilde{a}_a \\ \tilde{a}_1 \\ \tilde{a}_2 \\ \tilde{a}_3 \\ \tilde{a}_4 \end{pmatrix} = \begin{pmatrix} 1 & -C_{a1} & -Ca1 & -C_{a3} & C_{a3} \\ -C & 1 & -C_{12} & 0 & 0 \\ C_{1a} & -C_{12} & 1 & 0 & 0 \\ -C_{3a} & 0 & 0 & 1 & -C_{34} \\ C_{3a} & 0 & 0 & -C_{34} & 1 \end{pmatrix}^{-1} \cdot \begin{pmatrix} a_a \\ a_1 \\ a_2 \\ a_3 \\ a_4 \end{pmatrix}. \quad (6)$$

On taking the matrix inverse we find that the determinant of the matrix is given by:

$$\Delta = \frac{2G_{al}{}^2}{\omega - \omega_{ql} + i\Gamma/2} + \frac{2G_{au}{}^2}{\omega - \omega_{qu} + i\Gamma/2} - (\omega - \omega_a + i\Gamma/2) \quad (7)$$

where $\omega_{ql} = \omega_l + G_l$ is the quadrupole resonance associated with the coupling G_l between the lower pair of nanorods, and likewise $\omega_{qu} = \omega_u + G_u$ is the quadrupole resonance for the upper pair. The transmission spectrum is proportional to $I_{max} - A_a{}^2/|\Delta|^2$ so that the maxima and minima in the determinant determine the respective minima and maxima in the transmission spectrum. As shown in Fig. 8 this expression fits the experimental data very well. A further analysis of the expression for the determinant yields an approximate expression for the resonant frequencies which enables identification of the key factors that control each feature in the scattering spectrum.[38]

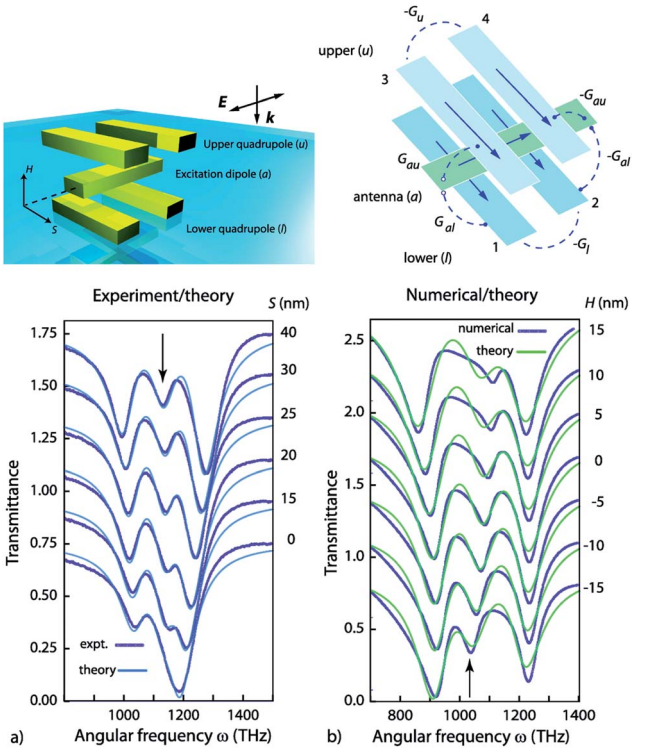

Fig. 8 (Top left) 3D plasmonic ruler (top right) inter-particle interactions (bottom) (a) experimental data from Liu *et al.*[60] and our analytical model fitted to the data for different lateral translations *S* of the antenna; (b) numerical data and fits of our analytical model for different vertical displacements *H* of the antenna (reproduced with permission from the American Chemical Society[38]).

Challenges

We have developed a conceptual platform that allows for a rational design of plasmonic structures and we have presented a few case studies that illustrate both its simplicity and applicability. Plasmonic assemblies are emerging as a new class of metamaterials with enormous potential for novel opto-electronic technologies, enhanced photo-voltaic devices and photo-catalysis. The next big step with this simple conceptual platform is the formulation of a *multiphysics* approach that incorporates the EEM to enable the design of plasmonic assemblies with, for instance, targeted photo-thermal properties[61] or for hot-electron injection.[62]

As clearly evidenced by the case studies presented here, a key feature of realising "plasmonics by design" is to create plasmonic nanoparticle assemblies with targeted geometrical arrangements. To date, top-down electron beam lithography (EBL) is the most accurate experimental approach for achieving this level of control. However, there are some open problems with EBL, which include:

- The required physical vapour deposition of metals results in non-crystalline structures, which is known to introduce imperfections that increase the plasmon resonance linewidth by means of non-elastic scattering.
- The resolution achievable with EBL is >5 nm.[63] Due to the evanescent nature of surface plasmon modes, strongest coupling is expected to occur at very short inter-particle distances.
- EBL is not a realistic technique for scaling up the production of nanoparticle assemblies of controlled geometry, due to its high cost and relatively low writing speed.

The first limitation has long been overcome by the chemical synthesis of nanoparticles. With respect to the other two

limitations, significant steps have been made. In particular, bottom-up fabrication of complex assemblies using different self-assembly techniques is now possible,[23] but it seems that much of these approaches cannot be easily extrapolated for producing assemblies of controlled geometries *with particles of high aspect ratio.* In this respect, the use of molecular templates, such as DNA origami,[64] has recently been shown to be a promising alternative capable of producing 3D plasmonic assemblies with metal nanorods, in amounts similar to Avogadro's number.[64] However, like most other wet-chemical approaches reported to date, the molecular template route results in a collection of random structures with many different configurations. Therefore an existing challenge in the materials chemistry of plasmonic assemblies is the development of self-assembly techniques that, in addition to producing large amounts of these assemblies, have high selectivity towards a specific geometrical configuration.

This work was performed in part at and partially supported by the Melbourne Centre for Nanofabrication (MCN) in the Victorian Node of the Australian National Fabrication Facility (ANFF). D.E.G. would like to thank the ARC for support through a Discovery Project DP110101767. D.E.G. and T.J.D. acknowledge the ANFF for support through MCN Technology Fellowships. A.M.F. would like to thank the ARC for support through a Future Fellowship FT110100545 as well as DP120101573.

References

1 N. J. Halas, *Nano Lett.*, 2010, **10**, 3816.
2 L. M. Liz-Marzán, *J. Phys. Chem. Lett.*, 2013, **4**, 1197.
3 T. W. Odom and G. C. Schatz, *Chem. Rev.*, 2011, **111**, 3667.
4 X. Guo, *J. Biophotonics*, 2012, **5**, 483.
5 H. Atwater and A. Polman, *Nat. Mater.*, 2010, **9**, 205.
6 X. Zhang, Y. L. Chen, R.-S. Liu and D. P. Tsai, *Reports on Progress in Physics*, 2013, **76**, 046401.
7 P. Christopher, H. Xin, A. Marimuthu and S. Linic, *Nat. Mater.*, 2012, **11**, 1044.
8 O. Neumann, C. Feronti, A. D. Neumann, A. Dong, K. Schell, B. Lu, E. Kim, M. Quinn, S. Thompson, N. Grady, P. Nordlander, M. Oden and N. J. Halas, *Proc. Natl. Acad. Sci. U. S. A.*, 2013, **110**, 11677.
9 L. R. Hirsch, R. J. Stafford, J. A. Bankson, S. R. Sershen, B. Rivera, R. E. Price, J. D. Hazle, N. J. Halas and J. L. West, *Proc. Natl. Acad. Sci. U. S. A.*, 2003, **100**, 13549.
10 E. C. Dreaden and M. A. El-Sayed, *Acc. Chem. Res.*, 2012, **45**, 1854.
11 M. Moskovits, *Rev. Mod. Phys.*, 1985, **57**, 783.
12 A. G. Curto, G. Volpe, T. H. Taminiau, M. P. Kreuzer, R. Quidant and N. F. van Hulst, *Science*, 2010, **329**, 930.
13 N. Liu, W. Qin, G. Qin, T. Jiang and D. Zhao, *Chem. Commun.*, 2011, **47**, 7671.
14 M. Kauranen and A. V. Zayats, *Nat. Photonics*, 2012, **6**, 737.
15 R. H. Ritchie, *Phys. Rev.*, 1957, **106**, 874.
16 U. Kreibig and M. Vollmer, *Optical properties of metal clusters*, Springer series in materials science 25, Springer – Verlag, Berlin, 1995, UniM Chem 546.3 KREI.
17 S. Maier, *Plasmonics: fundamentals and applications*, Springer, New York, 2007.
18 C. Sönnichsen, T. Franzl, T. Wilk, G. von Plessen, J. Feldmann, O. Wilson and P. Mulvaney, *Phys. Rev. Lett.*, 2002, **88**, 077402.
19 M. W. Knight, H. Sobhani, P. Nordlander and N. J. Halas, *Science*, 2011, **332**, 702.
20 J.-S. Huang, V. Callegari, P. Geisler, C. BrÃning, J. Kern, J. C. Prangsma, X. Wu, T. Feichtner, J. Ziegler, P. Weinmann, M. Kamp, A. Forchel, P. Biagioni, U. Sennhauser and B. Hecht, *Nat. Commun.*, 2010, **1**, 150.
21 H. Ditlbacher, A. Hohenau, D. Wagner, U. Kreibig, M. Rogers, F. Hofer, F. R. Aussenegg and J. R. Krenn, *Phys. Rev. Lett.*, 2005, **95**, 257403.
22 B. J. Wiley, D. J. Lipomi, J. Bao, F. Capasso and G. M. Whitesides, *Nano Lett.*, 2008, **8**, 3023, PMID: 18720977.
23 S. J. Barrow, A. M. Funston, X. Wei and P. Mulvaney, *Nano Today*, 2013, **8**, 138.
24 J. Zuloaga, E. Prodan and P. Nordlander, *Nano Lett.*, 2009, **9**, 887, PMID: 19159319.
25 A. M. Funston, C. Novo, T. J. Davis and P. Mulvaney, *Nano Lett.*, 2009, **9**, 1651.
26 V. Myroshnychenko, J. Rodriguez-Fernandez, I. Pastoriza-Santos, A. M. Funston, C. Novo, P. Mulvaney, L. M. Liz-Marzan and F. J. G. de Abajo, *Chem. Soc. Rev.*, 2008, **37**, 1792.
27 E. M. Purcell and C. R. Pennypacker, *Astrophys. J.*, 1973, **186**, 705.
28 A. Taflove, S. Hagness, *et al.*, *Computational electrodynamics: the finite-difference time-domain method*, Artech House, (2000).
29 F. J. García de Abajo and A. Howie, *Phys. Rev. B: Condens. Matter Mater. Phys.*, 2002, **65**.
30 U. Hohenester and J. Krenn, *Phys. Rev. B: Condens. Matter Mater. Phys.*, 2005, **72**, 195429.
31 E. Prodan, C. Radloff, N. J. Halas and P. Nordlander, *Science*, 2003, **302**, 419.
32 I. D. Mayergoyz, Z. Zhang and G. Miano, *Phys. Rev. Lett.*, 2007, **98**, 147401.
33 I. D. Mayergoyz, D. R. Fredkin and Z. Zhang, *Phys. Rev. B: Condens. Matter Mater. Phys.*, 2005, **72**, 155412.
34 T. J. Davis, K. C. Vernon and D. E. Gómez, *Opt. Express*, 2009, **17**, 23655.
35 T. J. Davis, D. E. Gómez and K. C. Vernon, *Nano Lett.*, 2010, **10**, 2618.
36 T. J. Davis, K. C. Vernon and D. E. Gómez, *Phys. Rev. B: Condens. Matter Mater. Phys.*, 2009, **79**, 155423; Also in: *Vir. J. Nan. Sci. & Tech*, 2009, **19**, 17.
37 D. E. Gómez, K. C. Vernon and T. J. Davis, *Phys. Rev. B: Condens. Matter Mater. Phys.*, 2010, **81**, 075414.
38 T. J. Davis, M. Hentschel, N. Liu and H. Giessen, *ACS Nano*, 2012, **6**, 1291.
39 S. J. Barrow, A. M. Funston, D. E. Gómez, T. J. Davis and P. Mulvaney, *Nano Lett.*, 2011, **11**, 4180.
40 K. C. Vernon, A. M. Funston, C. Novo, D. E. Gómez, P. Mulvaney and T. J. Davis, *Nano Lett.*, 2010, **10**, 2080.
41 T. J. Davis and E. Hendry, *Phys. Rev. B: Condens. Matter Mater. Phys.*, 2013, **87**, 085405.

42 F. Eftekhari and T. J. Davis, *Phys. Rev. B: Condens. Matter Mater. Phys.*, 2012, **86**, 075428.

43 A. Djalalian-Assl, D. E. Gómez, A. Roberts and T. J. Davis, *Opt. Lett.*, 2012, **37**, 4206.

44 T. J. Davis, D. E. Gómez and K. C. Vernon, *Phys. Rev. B: Condens. Matter Mater. Phys.*, 2010, **81**, 045432; Also in: *Vir. J. Nan. Sci. & Tech*, 2010, **21**(7).

45 T. J. Davis, D. E. Gómez and K. C. Vernon, *Phys. Rev. B: Condens. Matter Mater. Phys.*, 2010, **82**, 205434.

46 D. E. Gómez, A. Roberts, T. J. Davis and K. C. Vernon, *Phys. Rev. B: Condens. Matter Mater. Phys.*, 2012, **86**, 035411.

47 D. E. Gómez, Z.-Q. Teo, M. Altissimo, T. Davis, S. Earl and A. Roberts, *Nano Lett.*, 2013, **13**, 3722.

48 M. W. Knight, Y. Wu, J. B. Lassiter, P. Nordlander and N. J. Halas, *Nano Lett.*, 2009, **9**, 2188.

49 C. Novo, A. M. Funston, I. Pastoriza-Santos, L. M. Liz-Marzan and P. Mulvaney, *J. Phys. Chem. C*, 2008, **112**, 3.

50 T. Tamaguchi, S. Toshia and A. Kinbara, *Thin Solid Films*, 1974, **21**, 173.

51 J. Kumar, X. Wei, S. Barrow, A. M. Funston, K. G. Thomas and P. Mulvaney, *Phys. Chem. Chem. Phys.*, 2013, **15**, 4258–4264.

52 S. J. Barrow, A. M. Funston, X. Wei and P. Mulvaney, *Nano Today*, 2013, **8**, 138.

53 J. A. Fan, C. Wu, K. Bao, J. Bao, R. Bardhan, N. J. Halas, V. N. Manoharan, P. Nordlander, G. Shvets and F. Capasso, *Science*, 2010, **328**, 1135.

54 J. A. Fan, Y. He, K. Bao, C. Wu, J. Bao, N. B. Schade, V. N. Manoharan, G. Shvets, P. Nordlander, D. R. Liu and F. Capasso, *Nano Lett.*, 2011, **11**, 4859.

55 A. M. Funston, T. J. Davis, C. Novo and P. Mulvaney, *Philos. Trans. R. Soc., A*, 2011, **369**, 3472.

56 S. J. Barrow, X. Wei, J. S. Baldauf, A. M. Funston and P. Mulvaney, *Nat. Commun.*, 2013, **3**, 1275.

57 C. Novo, A. M. Funston, I. Pastoriza-Santos, L. L. Liz-Marz'an and P. Mulvaney, *Angew. Chem., Int. Ed.*, 2007, **46**, 3517.

58 A. M. Funston, D. E. Gómez, M. Karg, K. C. Vernon, T. J. Davis and P. Mulvaney, *J. Phys. Chem. Lett.*, 2013, **4**, 1994.

59 A. F. Cotton, *Chemical Applications of Group Theory*, Wiley-Interscience, 3rd edn, 1990.

60 N. Liu, M. Hentschel, T. Weiss, A. P. Alivisatos and H. Giessen, *Science*, 2011, **332**, 1407.

61 A. O. Govorov and H. H. Richardson, *Nano Today*, 2007, **2**, 30.

62 A. O. Govorov, H. Zhang and Y. K. Gun'ko, *J. Phys. Chem. C*, 2013, **117**, 16616.

63 M. S. M. Saifullah, T. Ondarçuhu, D. K. Koltsov, C. Joachim and M. E. Welland, *Nanotechnology*, 2002, **13**, 659.

64 X. Lan, Z. Chen, G. Dai, X. Lu, W. Ni and Q. Wang, *J. Am. Chem. Soc.*, 2013, **135**, 11441.

65 P. B. Johnson and R. W. Christy, *Phys. Rev. B: Solid State*, 1972, **6**, 4370.

66 More explicitly, the size d of the nanoparticle assembly should satisfy $2\pi d/\lambda = 1$, where λ is the wavelength of light.

67 We make use of the Mulliken notation for the irreducible representations.